

Tree Crown Detection on Multispectral VHR Satellite Imagery

Ioannis N. Daliakopoulos, Emmanouil G. Grillakis, Aristeidis G. Koutroulis, and Ioannis K. Tsanis

Abstract

A new method called *Arbor Crown Enumerator (ACE)* was developed for tree crown detection from multispectral Very High-resolution (VHR) satellite imagery. ACE uses a combination of the Red band and Normalized Difference Vegetation Index (NDVI) thresholding, and the Laplacian of the Gaussian (LOG) blob detection method. This method minimizes the detection shortcomings of its individual components and provides a more accurate estimation of the number of tree crowns captured in an image sample. The ACE was applied successfully to sample images taken from a four-band QuickBird ($0.7\text{m} \times 0.7\text{m}$) scene of Keritis watershed, in the Island of Crete. The method performs very well for different tree types, sizes and densities that may include non vegetation features such as roads and houses. Statistical analysis on the tree crown detection results from the sample images supports the agreement between the measurements and the simulations. The new method reduces considerably the effort of manual tree counting and can be used for environmental applications of fruit orchard, plantation and open forest population monitoring.

Introduction

Reducing uncertainty in land-use mapping is very important in water resources, agriculture and forestry management. This has also been obvious in decision making tier with the European commission spending 170USD (120€) million on a tree counting system which was deemed necessary to record the condition and number of trees (Moore, 2006). The main purpose of the survey was to establish a regulatory register, thus providing a basis for management and control of the financial aid to farmers (Kay *et al.*, 1997). The parcel-level requirement for data from areas with complex agronomic characteristics demands an approach that can define individual trees. (Karantzalos and Argialas, 2004).

The knowledge of plant distribution per farm can be also used for irrigation water prices and availability regulation, according to individual farmer needs. In order to cross reference farmer statements on the number of irrigated trees, an automated tree counting technique can be used. Combined with land-cover classification or segmentation

algorithms this can result to a very useful product for water resources managing authorities.

Keeping a dynamically updated inventory or tracking the number of trees through time can be used to trace the fate of individual trees. This can be a very important index when associated with diseases, weather conditions, and ecosystem behavior. Especially for endangered or protected areas that are difficult to manage, a dynamically updated, high-resolution product can prevent disasters from spreading. Furthermore, tree counting results can be coupled with hazard management models such as forest fires models (Lasaponara and Lanorte, 2007a; Lasaponara and Lanorte, 2007b; Loboda and Csiszar, 2007) to produce accurate results. Minimizing uncertainties can also help understand many ecosystem processes ranging in scale, from biomass equivalent and regional fuel loading for fire risk assessments (Pyne *et al.*, 1996) to global climate models (Post, 1993).

Vegetation units have traditionally been extracted through visual interpretation and manual digitizing of large scale aerial photographs (Dralle and Rudemo, 1997, Larsen and Rudemo, 1998, Tarp-Johansen, 2002, Freeman and Buck, 2003, Pauleit *et al.*, 2005). This technique, although efficient for detailed mapping, is time consuming and may be largely impractical (Mathieu *et al.*, 2007). Until recently, the spatial resolution of satellite sensors has been too coarse (e.g., 30 or 20 m for Landsat or SPOT) to be appropriate for application, given the size of a tree crown. The last generation of high-resolution Earth Observation satellites, e.g., Ikonos or QuickBird, provides images with a level of detail compatible with urban mapping (Jensen and Cowen, 1999), i.e., from 0.6 to 2.5 m spatial resolution and can thus provide data at a level appropriate for tree detection. In addition, multispectral sensors have the advantage of recording near infrared (NIR) radiation which is the most sensitive spectral band used to map vegetation canopy properties (Guyot, 1990).

In more recent work, Song and Woodcock (2003), present a simple analytical model to estimate tree crown size using sills of semi-variograms from images at two spatial resolutions. On a later approach, Song (2007) explores the potential of using spatial information of high-resolution optical imagery for estimating mean tree crown diameter on a stand basis with a panchromatic Ikonos image. Gougeon and Leckie (2006) give an assessment of the effects of different spatial resolutions on the detection, delineation, and classification of the individual tree crowns on Ikonos images using a valley-following

Ioannis N. Daliakopoulos, Emmanouil G. Grillakis, and Aristeidis G. Koutroulis are with the Department of Environmental Engineering, Technical University of Crete, 73100 Chania, Greece.

Ioannis K. Tsanis is with the Department of Environmental Engineering, Technical University of Crete, 73100 Chania, Greece, on leave from the Department of Civil Engineering, McMaster University, Canada (tsanis@hydromech.gr).

Photogrammetric Engineering & Remote Sensing
Vol. 75, No. 10, October 2009, pp. 1201–1211.

0099-1112/09/7510-1201/\$3.00/0
© 2009 American Society for Photogrammetry
and Remote Sensing

algorithm and a rule-based isolation module were applied to delineate the individual tree crowns. Song and Dickinson (2008) found that the spatial properties of Ikonos panchromatic imagery are highly valuable in estimating both tree crown size and LAI. Ozdemir (2008) investigates the relationship between field-measured stem volume and tree attributes, including tree crown area and tree shadow area, measured from pan-sharpened QuickBird imagery using visual delineation and computer-aided automatic classification methods

In September 1997, the European Commission (Directorate General of Agriculture) launched the “OLISTAT” project, supported by the Joint Research Centre (JRC) (Masson, 2005), with the goal to estimate the number of olive trees in France, Italy, Spain, Portugal, and Greece. A prototype tool, OLICOUNT (Kay *et al.*, 1998) is based on a combination of image threshold (i.e., using the spectral characteristics of trees), region growing, and tests based on tree morphological parameters (i.e., using the morphology of individual trees). More details on the method can be found in Peedel *et al.* (2000). The OLICOUNT software has various limitations, as it was originally designed for olive trees, and it was not tested for other fruit trees or with image resolutions of less than 1 m. Nevertheless, OLICOUNT was adapted to support VHR images, and the JRC carried out some tests with other fruit trees species (nuts and citrus). For the moment, OLICOUNT works only with single-band images and 16-bit support was added following Version 2.0 (Bagli, 2005). Therefore, analysis of multispectral images would require a different approach (Masson, 2005).

Methodology

Red Band Thresholding

The Photosynthetically Active Radiation (PAR) or Visible Red (RED: 630 to 690 nm) is a chlorophyll absorption band important for vegetation classification. Live green plants absorb solar radiation in the PAR spectral region, which they use as a source of energy in the process of photosynthesis (Gates, 1980). For this reason, the RED band portion of a multispectral satellite image appears dark where green plants are captured.

A method proposed by Tsanis and Seiradakis (2002, also included in Tsanis *et al.*, 2006) takes advantage of this property of chlorophyll absorption in order to count tree crowns from a high-resolution satellite image. Eleven-bit QuickBird images contain a pixel value range from 0 to 2047 and are usually scaled and stored as 16-bit. When thresholding the RED band against a single value, estimated tree-crowns appear as artifacts (Figure 1a). Artifacts can be then converted to topological polygons and at the center of each a tree crown is modeled as a point feature (Figure 1b). The choice of the appropriate value of threshold α for an image $f(x,y)$ so that:

$$g(x,y) = \begin{cases} 1 & \text{for } f(x,y) > \alpha \\ 0 & \text{for } f(x,y) < \alpha \end{cases}$$

will produce an estimate of the actual number of trees present in the sample.

Different values of thresholds are applied in the case shown in Figure 1a and are plotted against detected tree crowns in Figure 2. For threshold values under 100, the method still has not detected all features, and for values over 130, dense tree tops are being considered as single trees. From simple observations on the same site and product, values over 190 cluster most of the vegetation in one cell.

Tsanis and Seiradakis (2002) found that this simple method works well for threshold values of 120, but this is a

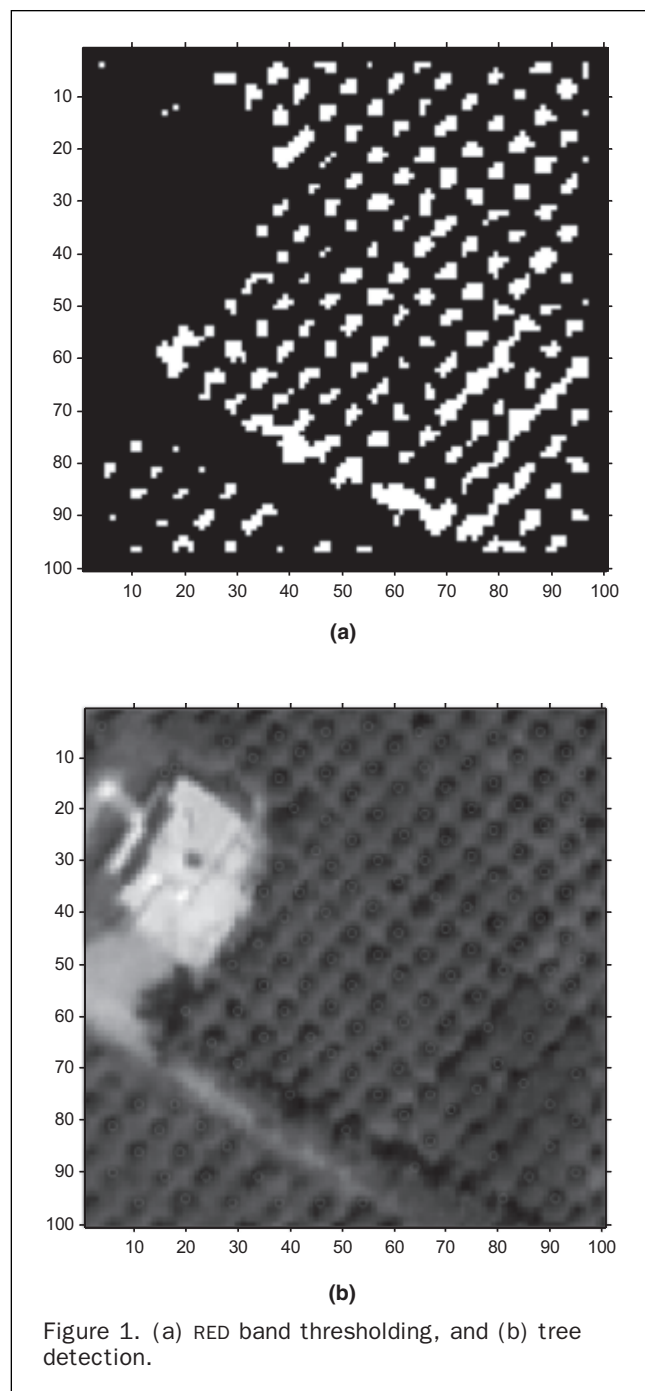


Figure 1. (a) RED band thresholding, and (b) tree detection.

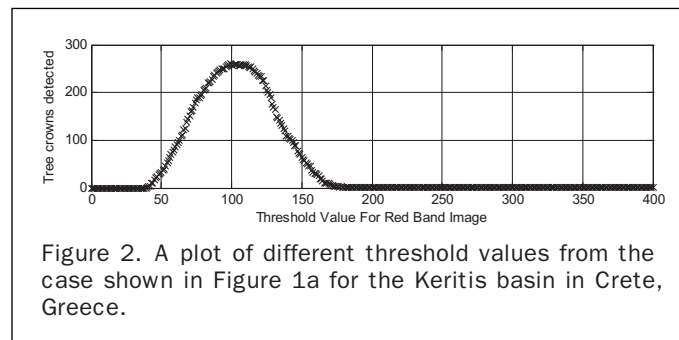


Figure 2. A plot of different threshold values from the case shown in Figure 1a for the Keritis basin in Crete, Greece.

site and satellite product-specific value. For different sites and satellite products this simple analysis has to be carried out in advance.

Blob Detection

One of the first and most common blob detectors is based on the Laplacian of the Gaussian. A given image $f(x,y)$ can be convolved by a Gaussian kernel h_g of width σ^2 :

$$h_g(x,y,\sigma) = \frac{1}{2\pi\sigma^2} e^{-(x^2+y^2)/2\sigma^2}$$

to give a representation:

$$L(x,y,\sigma) = h_g(x,y,\sigma) \cdot f(x,y).$$

Then, the Laplacian operator is computed:

$$\nabla^2 L = L_{xx} + L_{yy}$$

which usually results in strong positive responses for dark blobs of extent σ and strong negative responses for bright blobs of similar size. Practically, the image $f(x,y)$ is processed with a filter given by:

$$h(x,y,\sigma) = \frac{(x^2 + y^2 - 2\sigma^2)h_g(x,y,\sigma)}{2\pi\sigma^6 \sum_x \sum_y h_g(x,y,\sigma)}.$$

Figure 3 shows a 61×61 (randomly chosen for visualization) Laplacian of the Gaussian filter with a standard deviation $\sigma = 20$ and its contours.

NDVI

Leaf cells have evolved to scatter (i.e., reflect and transmit) solar radiation in the near-infrared (NIR: 760 to 900 nm) spectral region which carries approximately half of the total incoming solar energy. This happens because the energy level per photon in that domain is not sufficient to be useful to synthesize organic molecules: a strong absorption in NIR would only result in over-heating the plant and possibly damaging the tissues. Therefore, live green vegetation which appears relatively dark in the RED band also appears relatively bright in the NIR (Gates, 1980). Since early instruments

of Earth Observation, such as NASA's ERTS and NOAA's AVHRR, acquired data in the RED and NIR, scientists exploited the strong differences in plant reflectance in order to determine their spatial distribution in these satellite images. The NDVI is calculated from these measurements as follows:

$$NDVI = \frac{NIR - RED}{NIR + RED}.$$

Since the NDVI is merely a normalized difference, it carries only a fraction of the information available in the original spectral reflectance data. It is also sensitive to a number of perturbing factors including atmospheric composition, clouds (Putsay and Csiszár, 1997), soil moisture (Kimura, 2007), anisotropic light reflectance and sensor spectral effects. For these reasons it is mostly used only for qualitative estimations.

For each spectral band individually, spectral reflectance is a ratio of the reflected over the incoming radiation, hence it takes values between 0.0 and 1.0. Thus, by design, the NDVI itself varies between -1.0 and $+1.0$. Empirically, the NDVI of an area containing a dense vegetation canopy will tend to positive values (0.3 to 0.8), while clouds and snow fields will be characterized by negative values of this index. Soils generally exhibit a NIR spectral reflectance, somewhat larger than the RED, and thus tend to also generate rather small positive NDVI values between 0.1 to 0.2.

Arbor Crown Enumeration (ACE)

The Arbor Crown Enumeration (ACE) algorithm is based on the combination of the above three procedures (examining the high absorption of Red Band, tracking down visible blobs, and NDVI thresholding) as presented in Figure 4.

Intuitively, each calculation on its own will not produce satisfying results. The blob detection will detect all blobs regardless of their nature so many "non-green" small size objects like buildings will also be included in the count. On the other hand, both the NDVI and the RED band thresholding will produce filters where individual trees will not be discretised when planted densely. In order to test these presumptions the algorithm was broken into two parts, ACE₁ and ACE₂. The former method is based only on blob detection and NDVI thresholding whereas the latter includes all three procedures. These presumptions (later tested and proved valid) lead to the combination of the calculations into an all inclusive algorithm (ACE₂).

Criteria of Evaluation

When the number of trees N_{actual} within a given area (e.g., a single field) is known, the relative error e_r of a tree crown estimate $N_{estimate}$ is given by:

$$e_r = 100\% \times \frac{N_{estimate} - N_{actual}}{N_{actual}}.$$

Thus, for a perfect estimation ($N_{estimate} = N_{actual}$) the relative error e_r is equal to 0.0 percent. Relative errors for small fields are not representative for evaluating a tree counting method since inaccuracies can appear in areas that have not been accounted for. Therefore, a large sample of land parcels needs to be taken into account. For k such parcels of land, the total relative error E_r is given by:

$$E_r = 100\% \times \frac{\sum_{k=1}^{i=1} (N_{estimate}^i - N_{actual}^i)}{\sum_{k=1}^{i=1} N_{actual}^i}.$$

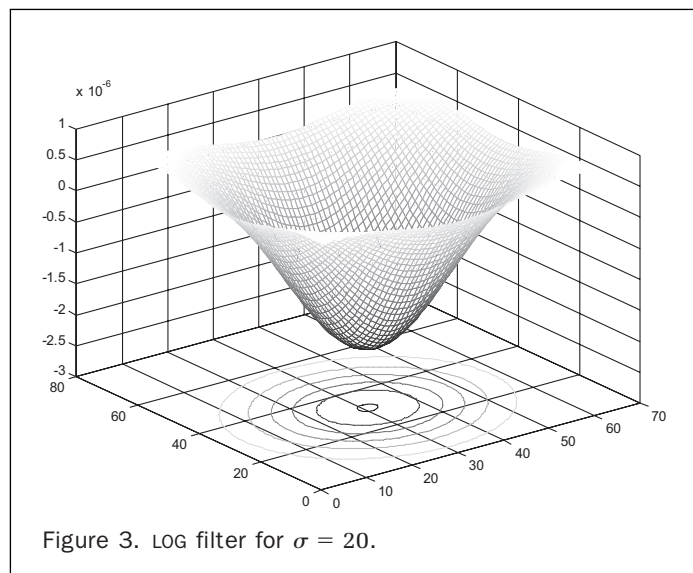


Figure 3. LOG filter for $\sigma = 20$.

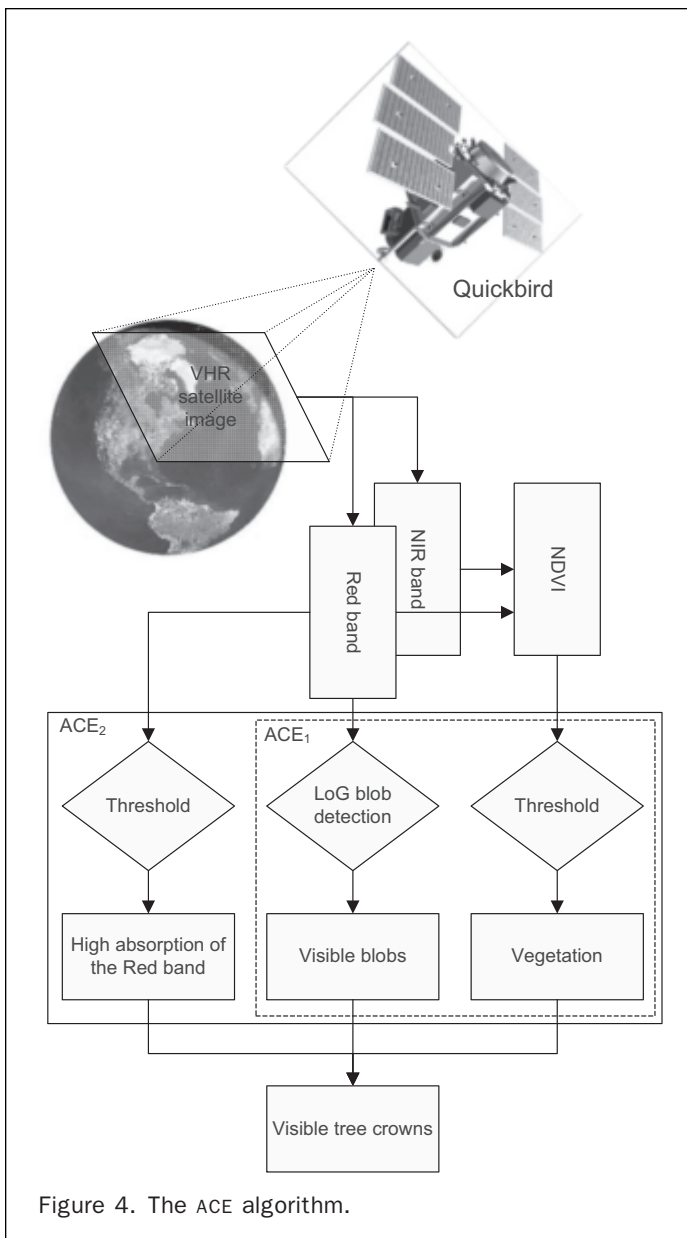


Figure 4. The ACE algorithm.

In reality, it is difficult to know the exact number of trees for a large area in order to make this comparison. Ideally, statistical methods should be applied over a representative sample (a collection of satellite image segments) of the population (total area covered). This sample has to include all the significant vegetation patterns that challenge a tree counting method, and at the same time, maintain the characteristics of the population. Nevertheless, population characteristics and method pitfalls are not known a priori. For this reason, the choice of the sample is based mostly on expert judgment and prior inference.

Case Study

Geographical Background

The Keritis hydrological basin is located between $35^{\circ} 15'$ to $35^{\circ} 32' N$ and $23^{\circ} 45'$ to $23^{\circ} 55' E$ on the island of Crete, Greece, 12 km west of the town of Chania (Figure 5). Starting from the White Mountains in its southernmost

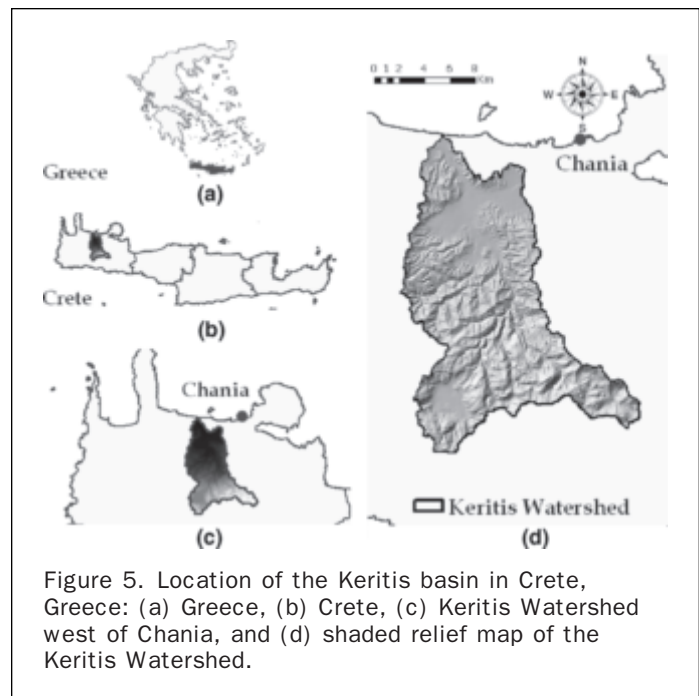


Figure 5. Location of the Keritis basin in Crete, Greece: (a) Greece, (b) Crete, (c) Keritis Watershed west of Chania, and (d) shaded relief map of the Keritis Watershed.

part, Keritis basin discharges into Platanias Bay in the north coast of Crete. The total area of the basin is 218 km^2 , and its altitude ranges from sea level to 2,355 m (mean altitude: 738 m).

From a hydrologic point of view, the Keritis basin is the most important watershed in the Prefecture of Chania (Soupios *et al.*, 2007). The water resources in the area are more than sufficient for this basin and are also used for public water supply and irrigation for the wider area. For this reason, the basin has been traditionally cultivated intensively with olive trees (*Olea europaea*, mainly cultivation of the cultivar *Koroneiki*), orange trees (*Citrus sinensis*), and vineyards (*Vitis vinifera*). Due to the large morphological diversity of the landscape, vegetation also varies from flat agriculturally exploited fields in the north to patches and shelves of olive trees mixed with short vegetation in the south. Other vegetation within the watershed includes oriental planes (*Platanus orientalis*) mostly along the stream banks and various herbs of the mint family (*Lamiaceae*) found mostly in the mountains.

Three satellite images, each covering a fraction of the basin, were taken by QuickBird on 02 May 2002 (Figure 6). The resolution of each image is $0.7 \text{ m} \times 0.7 \text{ m}$.

Calibration

Initially, the parameters of the method have to be calibrated by minimizing an error function. Generally, as in polynomial regression, the smaller the error during calibration the larger the chance of over-fitting the method to a specific sample. In reality, the goal is not a method that is perfectly accurate for a single sample, but one that is acceptably accurate for a large number of samples. Therefore, after trial and error, the error function optimum result is set to 10 percent which is a rather acceptable estimation for this type of application.

In order to perform calibration, a sample is taken from a known location where the trees have been counted in situ. Figure 7 shows a sample area of 100×100 pixels which includes 193 trees (typical pattern of orange cultivation).

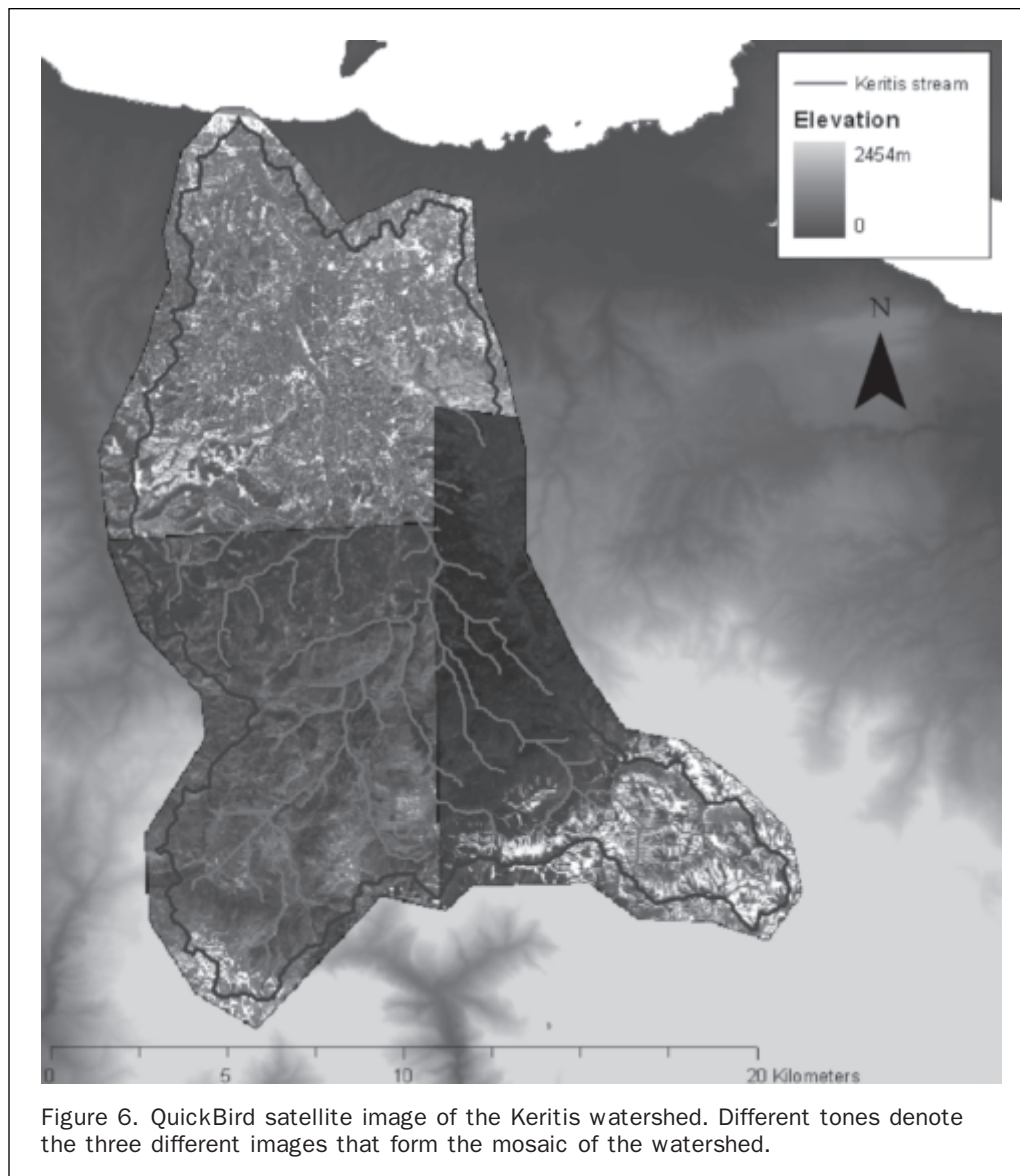


Figure 6. QuickBird satellite image of the Keritis watershed. Different tones denote the three different images that form the mosaic of the watershed.

This number does not take into account trees that are partially contained in the picture (e.g., on the fringe of the image) since they are not detected by ACE.

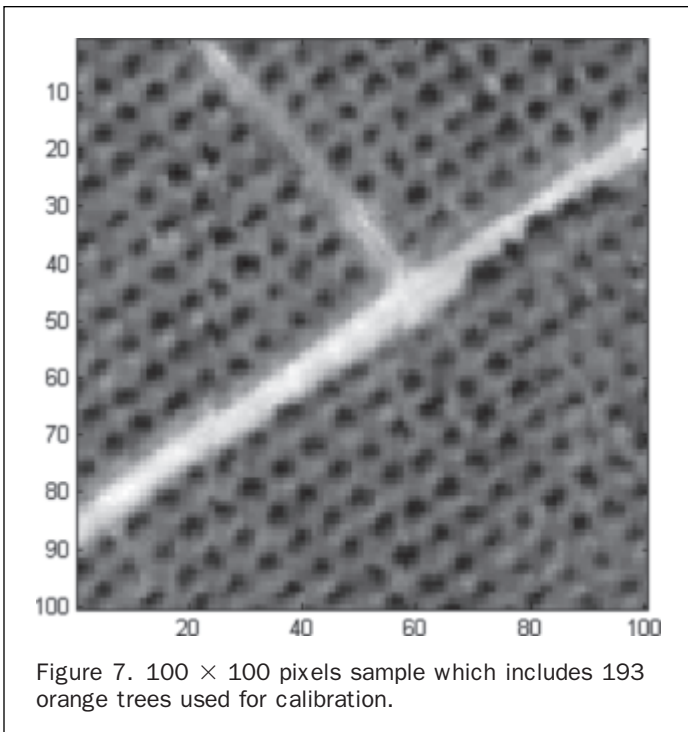
A search algorithm performs a tree-detection for a possible range of all ACE parameters. This way, candidate sets that fulfill the calibration goal can be singled out. Increasing the search pixel radius for the blob detection technique will result in trees that have a size smaller than this radius to be left out. Increasing the blob detection threshold will result into trees appearing less pronounced (having less contrast) to be ignored. Regarding NDVI, a large value cut-off will result in taking account of only those trees that have a strong NDVI signal. Figure 8 shows a visualization of the resulting values.

For the selected sample, the range of blob diameters that allow for a correct calculation of the tree numbers is six to eight pixels. For diameter values higher than eight pixels (5.6 m), the maximum number of detected trees is smaller than the actual number of trees. The most stable solutions appear for a diameter of eight pixels where the effect of threshold also becomes the least sensitive. For eight pixels, the range of solutions that successfully estimate the number

of trees can be achieved for a range of NDVI threshold values between 0.3 and 0.4.

The effect of threshold in blob detection ranging from 0.5 to 7 can be seen in Figure 9. With lower values, less pronounced blobs are also detected. For example, in Figure 9a on the north side of the dirt-road that runs across the sample picture, several blobs are detected where trees do not exist. On the other hand, high values can cause small trees not to be accounted for. For example, many relatively smaller or “fainter” trees have not been detected in the southeast of Figure 9b. Since we assume that the NDVI filter will later dispose of the blobs that do not represent vegetation, the goal of the threshold calibration should be to assign a large enough value so that insignificant vegetation like scrub and bush is not taken into account. For the tested case, the best results were accomplished for threshold values between 3.6 and 5.

Figure 10 shows the NDVI index for the selected image sample. Darker values (closer to zero) denote areas with no vegetation, e.g., along the dirt road that crosses the fields from southwest to northeast. The minor road that runs northwest is a low traffic agricultural path that allows for short vegetation



during spring (at the time the satellite image was taken). Therefore, its NDVI is comparably higher than that of the dirt road, and in Figure 10, it is practically not distinguishable from the fields. Thresholding the NDVI image will produce a filter that will leave out certain pixels. As shown in Figure 8, the sensitivity to NDVI changes is between 0.3 and 0.45, therefore the calibrated value has to be from this interval in order to have a better agreement with the actual data.

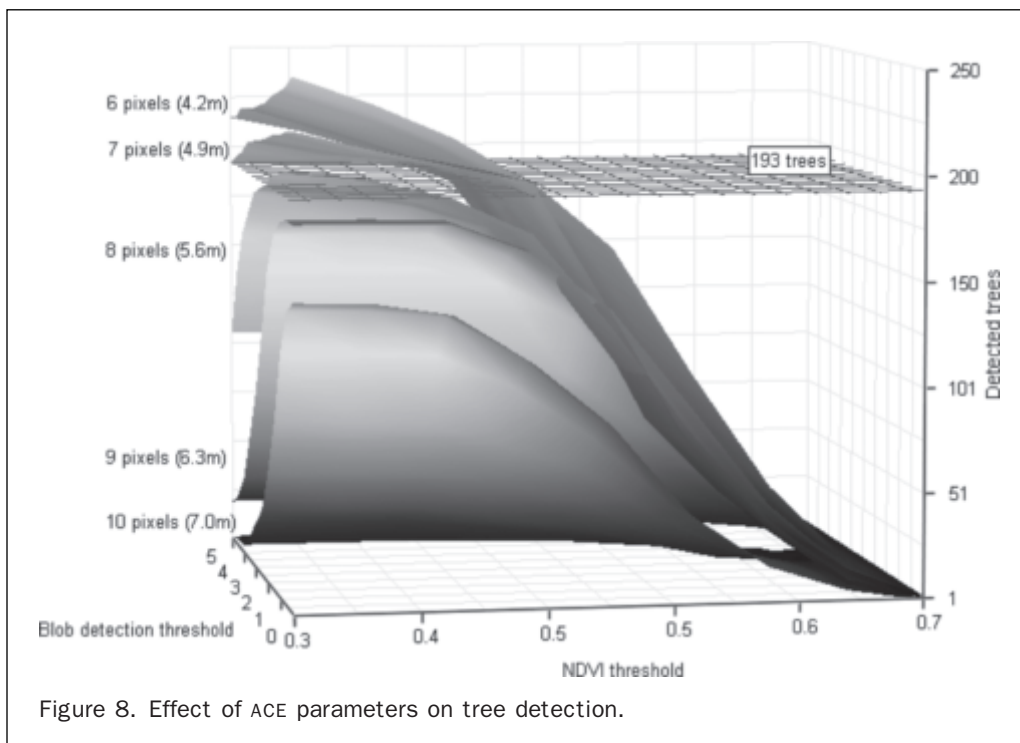
Figure 11 shows the effect of NDVI thresholding. For a low threshold value of 0.3, the discretization that takes place is only between the road and the vegetated fields (Figure 11a). Therefore, for values less than 0.3, practically all detected blobs will be considered as trees. For a high threshold value of 0.45 (Figure 11b), the NDVI filter will leave out more areas where the vegetation index has a weaker signal or soil is apparent. For a given pixel diameter and blob detection threshold, the NDVI effect can be seen in Figure 12.

Sensitivity analysis on possible combinations of blob detection and NDVI threshold values, reveals that the values 4.8 and 0.37, respectively are the ones that give the best fit to the actual number of trees. Figure 13 shows the resulting tree crown count.

Results and Discussion

Following the initial calibration process, the method was tested on ten different samples from the satellite image of the Keritis hydrological basin (Figure 14). The images were chosen with the objective to capture different tree sizes and densities as well as land-use and cultivation patterns in the watershed.

Table 1 shows the results acquired after performing four types of analysis on each sample image. Blob detection and simple RED band thresholding were performed separately in order to demonstrate their individual shortcomings. Even though RED band thresholding has a higher standard error than blob detection, this error is quite large to extract useful conclusions for a wider area. The blob detection method seems to overestimate the number of trees more often whereas RED band thresholding underestimates it. Therefore, both approaches are not sufficiently accurate to be used individually. The combination of algorithms denoted as ACE₁ leads to a smaller average e_r and an E_r which is acceptable with most individual errors averaging out. The best performance was



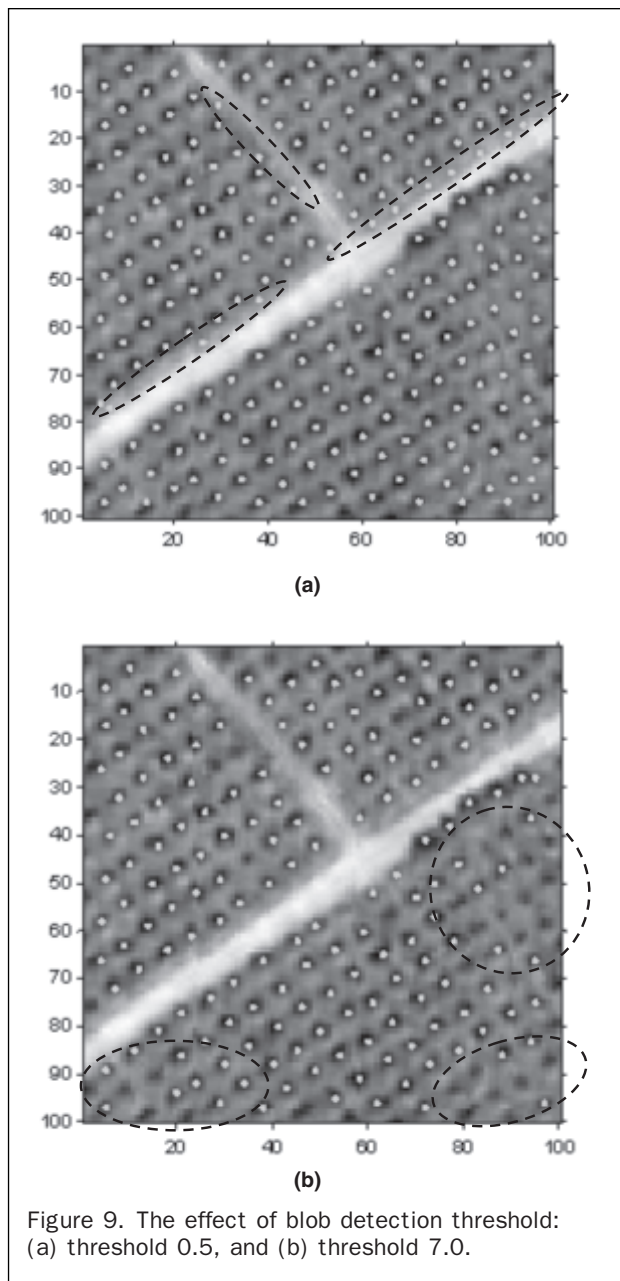


Figure 9. The effect of blob detection threshold: (a) threshold 0.5, and (b) threshold 7.0.

accomplished with ACE_2 . The final products of ACE_2 on the samples are shown in Figure 15.

In order to explain the merits and pitfalls of each method, individual sample results are analyzed giving greater gravity to those that result to larger errors.

For the samples SP01, SP09, and SP10 as is evident from Table 1, blob detection performs as good as the ACE_1 and ACE_2 methods. On the other hand, RED band thresholding greatly underestimates the number of trees. The reason for this is the high density of trees which leads RED band thresholding to cluster tree crowns. Here, the good results of blob detection overlap all other calculations and are the final product of ACE_1 and ACE_2 . In all three samples, NDVI filtering essentially produces a matrix of ones.

In the sample SP02, RED band thresholding also underestimates the actual number of trees whereas blob detection slightly overestimates it. Here, the difference of ACE_1 and

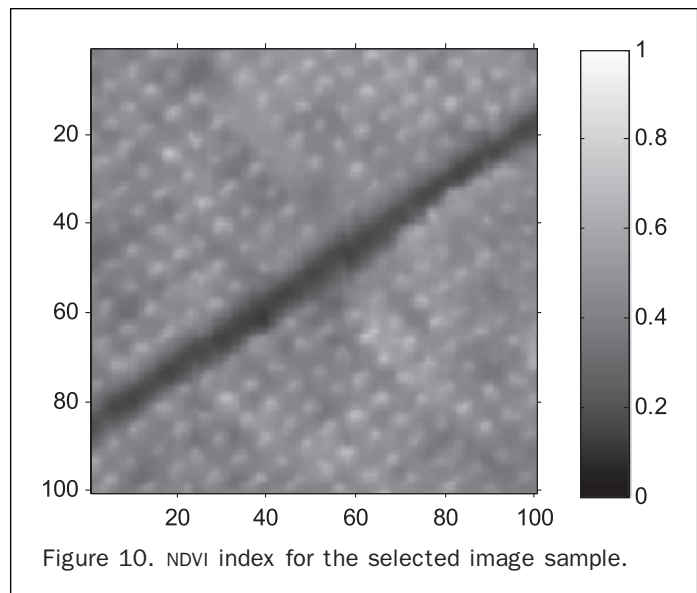


Figure 10. NDVI index for the selected image sample.

ACE_2 is apparent with the former detecting the same amount of trees as blob detection (217 from the actual 215) and the latter reducing them by 4. This is obviously where the RED band thresholding comes into play when moving from ACE_1 to ACE_2 .

Sample SP03 is the only case in which ACE_1 performs slightly better than ACE_2 . This can be attributed to the adverse effect of RED band thresholding failing to detect some of the trees that ACE_1 has captured. Apart from this fact all techniques have acceptable results. In sample SP04, due to a number of non-green artifacts (building and surrounding objects at the northwest side of the image) blob detection overestimates the total number of trees. These artifacts are cancelled out with the use of NDVI thresholding in ACE_1 , leaving few extra objects detected as trees. Finally, RED band thresholding improves the estimation. The fact that RED band thresholding scores a smaller absolute e_r is due to the clustering of dense vegetation mainly at the southwest part of the sample.

Similar to SP04 in sample SP05, the field on the east side of the sample presents artifacts that are spotted by the blob detection method without necessarily representing trees. Therefore, the number of trees is largely overestimated. Here, the difference between ACE_1 and ACE_2 is obvious, with the RED band thresholding capturing the difference between pasture land with short vegetation and shrubs (east part of the image) and tree vegetated land (west part of the image). The results of ACE_2 are very promising, detecting just four trees more than the actual number of trees.

Sample SP06 includes a non-vegetated parcel of land in the middle of an olive tree plantation. Blob detection and RED band thresholding give errors larger than 10 percent (16.2 percent and -10.4 percent, respectively) for the same reasons as in sample SP04 but ACE_2 dramatically improves the tree detection process missing just one tree.

Sample SP07 represents a very mixed landscape with artificial surfaces and vegetation of different size and shape. The main feature of vegetation is trees with multiple tops and various bushes. Blob detection overestimates the total tree number by almost 50 percent as it includes non-green objects, whereas RED band thresholding appears to have very good results. Nevertheless, the more complex algorithms fail

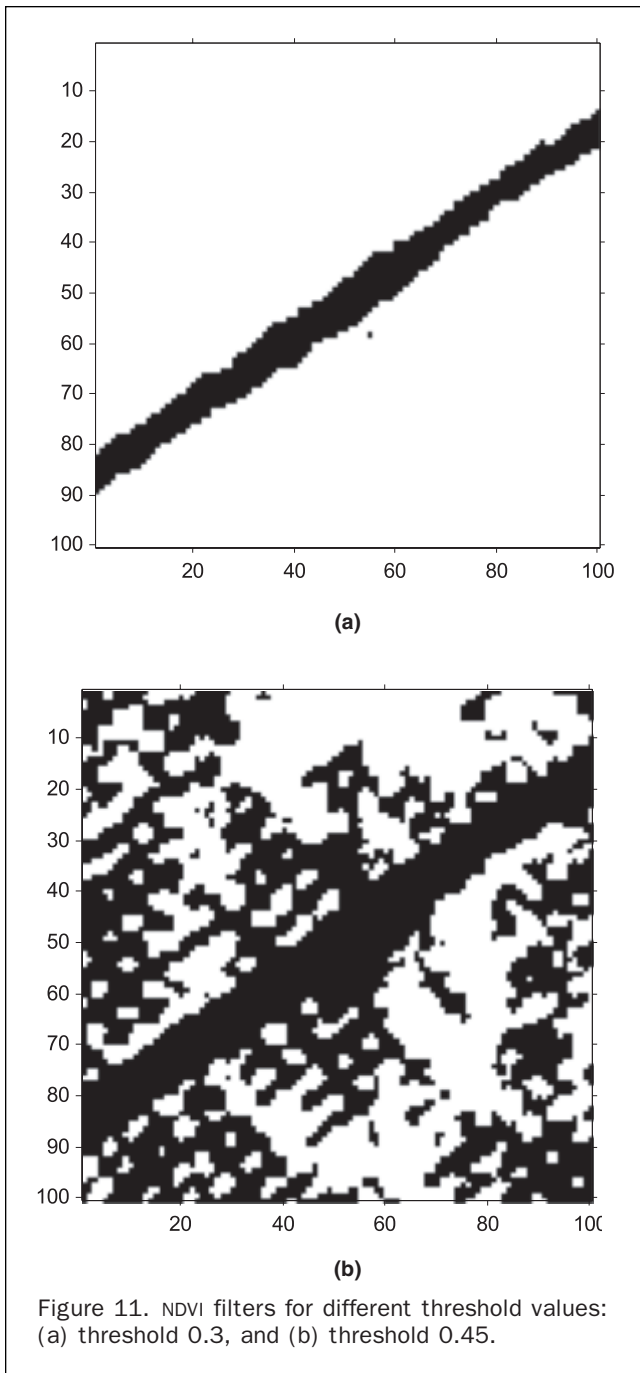


Figure 11. NDVI filters for different threshold values: (a) threshold 0.3, and (b) threshold 0.45.

with errors larger than 15 percent. The reason is obviously the poor match of NDVI calibration values, which is the

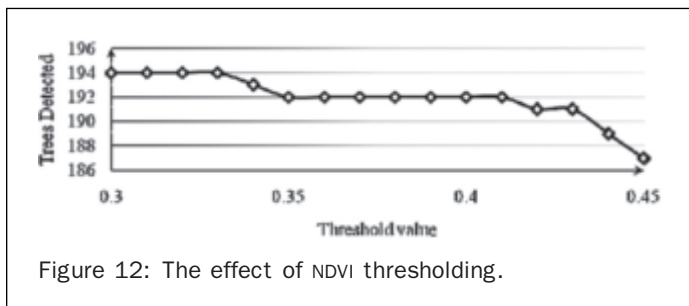
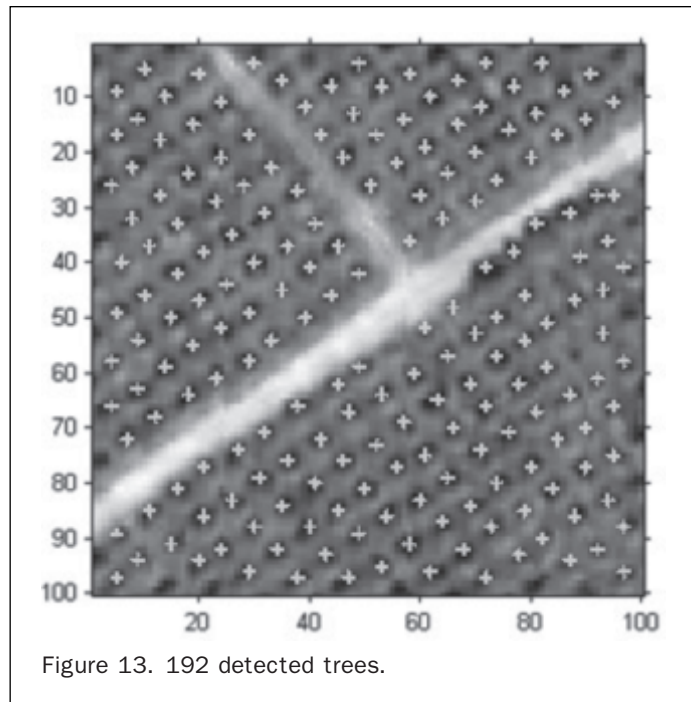


Figure 12: The effect of NDVI thresholding.

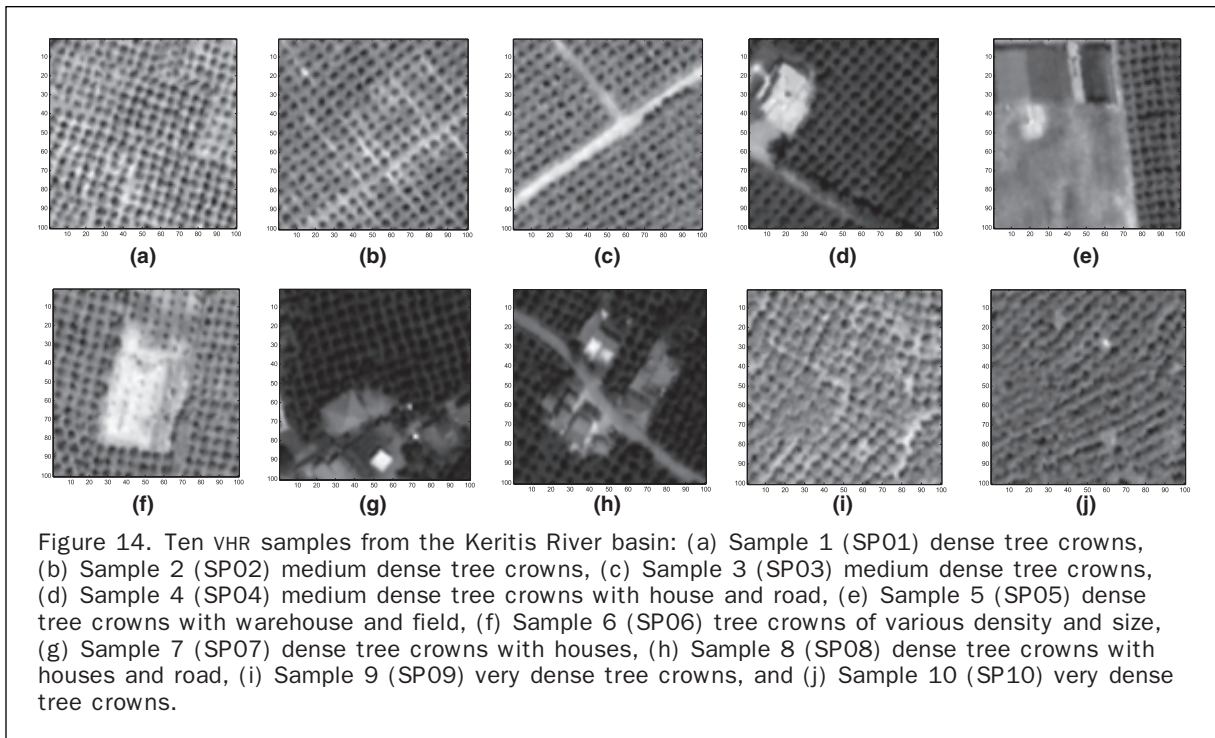


common element of ACE_1 and ACE_2 , except for the blob detection which is expected to fail in such cases. Specifically, some of the trees detected by these methods have not been considered “green enough,” and therefore have not been taken into account when counting trees in situ. This is normally not an issue and was expected since the NDVI threshold value was calibrated for a very different location. For a larger amount of samples it is expected that errors like this will be evened out towards a smaller total error.

As in SP07, sample SP08 involves a mixed landscape, and ACE_2 is able to distinguish between artificial surfaces and vegetation very well. Blob detection alone overestimates because of buildings and RED band thresholding underestimates due to clustered tree tops in several areas in the sample. Overall results for the ten sample images show that ACE_1 and ACE_2 increase the correlation coefficient from 0.35 and 0.59 to 0.87 and 0.92, respectively (Figure 16). Statistical analysis on the ACE_2 method produces a linear model $y = 0.8618x + 24.817$ where y is the estimated number of trees, and x is the number of measured trees, with a standard error of estimate $s_{y/x} = 13.398$ and a coefficient of determination $R^2 = 0.9209$. These results indicate that 92.09 percent of the original uncertainty has been explained by the linear model. At 95 percent confidence interval for this linear model, the intercept coefficient belongs to $[-12.95, 62.58]$, and slope belongs to $[0.656, 1.068]$. The desired values (0 for intercept and 1 for slope) fall within the intervals (Figure 16d) supporting the agreement between the measurements and the model.

Conclusions

The automatic extraction of features like tree crowns from VHR images requires validation in the field which is time consuming and ineffective for large areas. Existing tree crown detection methods such as blob detection, NDVI thresholding and RED band thresholding have shortcoming when applied individually. Blob detection detects all blob-like surfaces regardless if they represent vegetation or artificial objects. This usually leads to overestimations



in samples with mixed land-uses. RED band thresholding usually leads in tree crown clustering where vegetation is dense and therefore underestimates the actual number of trees. This method depends on the reflection values with which it has been calibrated and samples that belong to different satellite scenes have to be calibrated separately. This is also true for NDVI thresholding which is sensitive to a number of factors unique for each satellite image. Also, NDVI thresholding produces continuous filters where individual trees cannot be distinguished and is mostly used for qualitative estimations.

ACE has been designed to run with multispectral images (four bands: RGB + NIR) which carry more information than

a single band product. Therefore, instead of taking the strictly empirical approach of morphological classification, the problem is also solved physically using well documented vegetation indexes such as the NDVI and the absorption of the RED band by chlorophyll.

A combination of blob detection with NDVI thresholding using ACE_1 gives acceptable results for a selected number of samples where vegetation patterns do not differ much within the same image. The ACE_2 which also includes RED band thresholding gives the best results and this is attributed to the algorithm's ability to process multispectral images, which carry more information and to the complexity and combination of individual algorithms

TABLE 1. RESULTS FOR TREE COUNTING TECHNIQUES FOR TEN SAMPLE IMAGES

Sample Name	Measured number of trees	Blob detection		Red band Thresholding		ACE_1		ACE_2	
		Estimated trees	e_r	Estimated trees	e_r	Estimated trees	e_r	Estimated trees	e_r
SP01	248	244	-1.6%	206	-16.9%	244	-1.6%	244	-1.6%
SP02	215	217	0.9%	193	-10.2%	217	0.9%	213	-0.9%
SP03	193	197	2.1%	181	-6.2%	191	-1.0%	189	-2.1%
SP04	158	188	19.0%	148	-6.3%	178	12.7%	173	9.5%
SP05	74	169	128.4%	62	-16.2%	125	68.9%	78	5.4%
SP06	173	201	16.2%	155	-10.4%	185	6.9%	172	-0.6%
SP07	141	211	49.6%	143	1.4%	176	24.8%	165	17.0%
SP08	150	194	29.3%	118	-21.3%	151	0.7%	143	-4.7%
SP09	196	204	4.1%	121	-38.3%	204	4.1%	204	4.1%
SP10	226	196	-13.3%	80	-64.6%	196	-13.3%	196	-13.3%
Total number of trees	1,774	2,021		1,407		1,867		1,777	
E_r		13.9%		-20.7%		5.2%		0.2%	
Average e_r		23.5%		-18.9%		10.3%		1.3%	
e_r standard deviation		41.0%		19.3%		22.9%		8.3%	

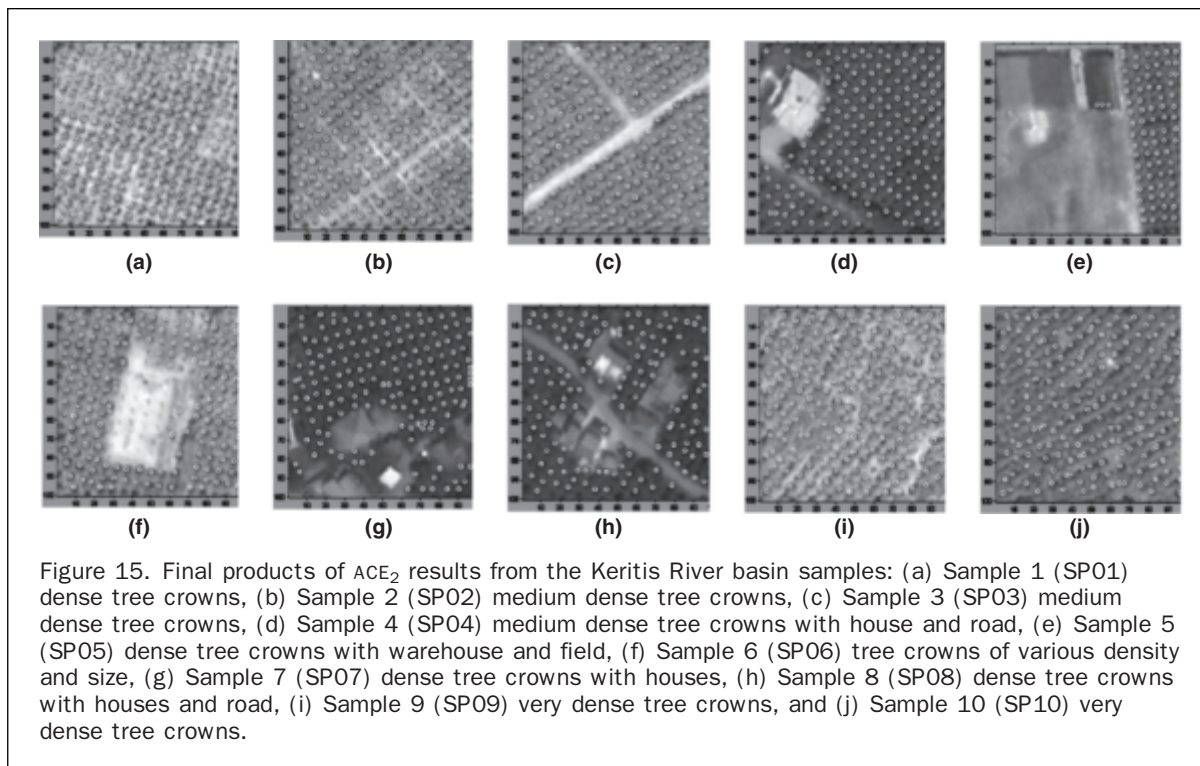


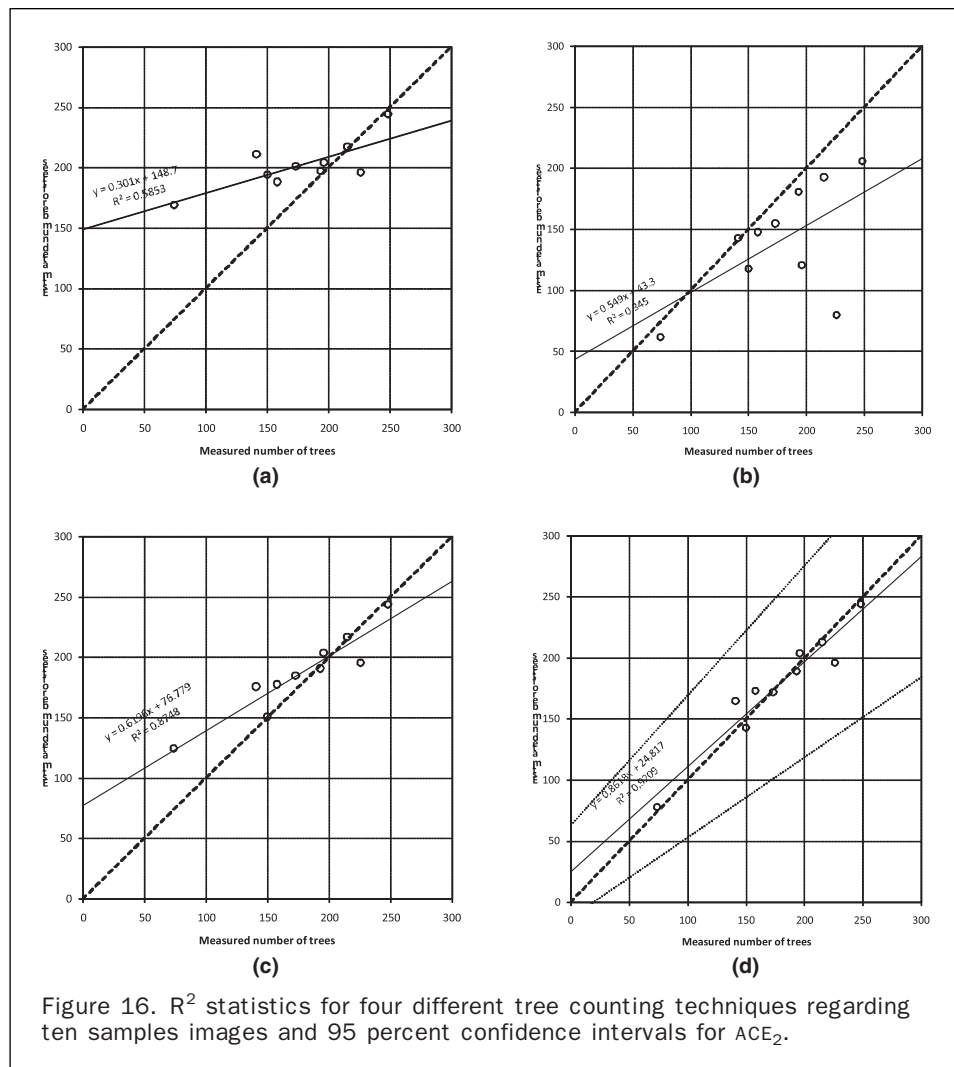
Figure 15. Final products of ACE₂ results from the Keritis River basin samples: (a) Sample 1 (SP01) dense tree crowns, (b) Sample 2 (SP02) medium dense tree crowns, (c) Sample 3 (SP03) medium dense tree crowns, (d) Sample 4 (SP04) medium dense tree crowns and road, (e) Sample 5 (SP05) dense tree crowns with house and field, (f) Sample 6 (SP06) tree crowns of various density and size, (g) Sample 7 (SP07) dense tree crowns with houses, (h) Sample 8 (SP08) dense tree crowns with houses and road, (i) Sample 9 (SP09) very dense tree crowns, and (j) Sample 10 (SP10) very dense tree crowns.

involved in the process. ACE₂ performs very well in distinguishing among land-uses, e.g., pastures, roads/dirt roads, building and trees (see SP03 to SP08 in Figure 15), and this can be contributed to the use of the RED band and NDVI filters. Also, its performance is not hindered much by differences in tree density or tree crown size due to use of blob detection (see SP01, SP02, and SP09, SP10 in Figure 15).

Finally the new tree crown detection method has been designed to detect a specific range of tree sizes rather than a specific tree type (as OLICOUNT). Therefore, it can have a wider range of applications, such as tree counting in complex vegetated and mixed land-use areas or forestry. The limits of application have to be defined in further research since counting tree populations in complex or dense forest strands might not be feasible. Also, a tree type classification module could be embedded in the future in order to expand its use in water resources management.

References

- Bagli, S., 2005. *OLICOUNT Software*, version 2.0, Technical Documentation.
- Dralle, K., and M. Rudemo, 1997. Automatic estimation of individual tree positions from aerial photos, *Canadian Journal of Forest Research*, 27:1728–1736.
- Freeman, C., and O. Buck, 2003. Development of an ecological mapping methodology for urban areas in New Zealand, *Landscape and Urban Planning*, 63(3):161–173.
- Gates, D.M., 1980. *Biophysical Ecology*, Springer-Verlag, New York, 611 p.
- Gougeon, F.A., and D.G. Leckie, 2006. The individual tree crown approach applied to Ikonos images of a coniferous plantation area, *Photogrammetric Engineering & Remote Sensing*, 72(11):1287–1297.
- Guyot, G., 1990, Optical properties of vegetation canopies, *Applications of Remote Sensing in Agriculture* (M.D. Steven and J.A. Clark, editors), Butterworth, London, pp. 19–43.
- Jensen, J.R., and D.C. Cowen, 1999. Remote sensing of urban/suburban infrastructure and socio-economic attributes, *Photogrammetric Engineering & Remote Sensing*, 65(5):611–622.
- Karantzalos, K., and D. Argialas, 2004. Towards the automatic olive trees extraction from aerial and satellite imagery, *International Archives of the Photogrammetry, Remote Sensing and Spatial Information Sciences*, 35(5):360–365, Istanbul, Turkey.
- Kay, S., O. Léo, J. Meyer-Roux, J. Delincé, and M. Van de Steene, 1997. Operational activities involving airborne remote sensing related to the Common Agricultural Policy, *Proceedings of the 3rd International Airborne Remote Sensing Conference and Exhibition*, 07–10 July, (ERIM International, Inc.), Copenhagen, Denmark, Vol. I, pp. 79–86.
- Kay, S., O. Léo, and S. Peedell, 1998. Space Applications Institute, JRC of the European Commission, *Proceedings of Commission VII, Working Group 4*, Ispra, Italy.
- Kimura, R., 2007. Estimation of moisture availability over the Liudaogou River basin of the Loess Plateau using new indices with surface temperature, *Journal of Arid Environments*, 70:237–252.
- Larsen, M., and M. Rudemo, 1998. Optimizing templates for finding trees in aerial photographs, *Pattern Recognition Letters*, 19(12):1153–1162.
- Lasaponara, R., and A. Lanorte, 2007a. Remotely sensed characterization of forest fuel types by using satellite ASTER data, *International Journal of Applied Earth Observation and Geoinformation*, 9:225–234.
- Lasaponara, R., and A. Lanorte, 2007b. On the capability of satellite VHR QuickBird data to fuel type characterization in fragmented landscape, *Ecological Modelling*, 204:79–84.
- Loboda, T.V., and I.A. Csizsár, 2007. Reconstruction of fire spread within wildland fire events in Northern Eurasia from the MODIS active fire product, *Global and Planetary Change*, 56:258–273.
- Masson, J., 2005. Use of very high-resolution airborne and spaceborne imagery: A key role in the management of olive, nuts and vineyard schemes in the frame of the common agricultural policy of the European Union, *Proceedings of Information and Technology for Sustainable Fruit and Vegetable Production, FRUTIC 05*, 12–16 September, Montpellier France.



- Mathieu, R., C. Freeman, and J. Aryal, 2007. Mapping private gardens in urban areas using object-oriented techniques and very high-resolution satellite imagery, *Landscape and Urban Planning*, 81(3):179–192.
- Moore, M., 2006. Living the high life on Europe's fraud coast, filed on 27 August 2006, URL: <http://www.telegraph.co.uk/news/1527387/Living-the-high-life-on-Europes-fraud-coast.html> (last date accessed: 11 July 2009).
- Ozdemir, I., 2008. Estimating stem volume by tree crown area and tree shadow area extracted from pan-sharpened QuickBird imagery in open Crimean juniper forests, *International Journal of Remote Sensing*, 29(19):5643–5655.
- Pauleit S., R. Ennos, and Y. Golding, 2005. Modeling the environmental impacts of urban land use and land cover change - A study in Merseyside, UK, *Landscape Urban Planning*, 71(2–4):295–310.
- Peedell, S., S. Kay, and G. Giordino, 2000. *Computer-assisted Recognition of Olive Trees in Digital Imagery*, Space Application Institute, Joint Research Center of Ispra, Italy.
- Post, W.M., 1993. Uncertainties in the terrestrial carbon cycle, *Vegetation Dynamics and Global Change* (A.M. Solomon and H.H. Shugart, editors), London, Chapman and Hall, pp. 116–132.
- Putsay, M., and I. Csiczár, 1997. Retrieval of surface reflectances from AVHRR visible and near-IR radiances, *Advanced Space Research*, 19(3):523–526.
- Pyne, S.J., P.L. Andrews, and R.D. Laven, 1996. *Introduction to Wildland Fire*, New York, Wiley and Sons.
- Song, C., and C.E. Woodcock, 2003. Estimating tree crown size from multiresolution remotely sensed imagery, *Photogrammetric Engineering & Remote Sensing*, 69(11):1263–1270.
- Song, C., 2007. Estimating tree crown size with spatial information of high-resolution optical remotely sensed imagery, *International Journal of Remote Sensing*, 28(15):3305–3322.
- Song, C., and M.B. Dickinson, 2008. Extracting forest canopy structure from spatial information of high-resolution optical imagery: tree crown size versus leaf area index, *International Journal of Remote Sensing*, 29(19):5605–5622.
- Soupios, P.M., M. Kouli, F. Vallianatos, A. Vafidis, and G. Stavroulakis, 2007. Estimation of aquifer hydraulic parameters from surficial geophysical methods: A case study of Keritis Basin in Chania (Crete-Greece), *Journal of Hydrology*, 338:122–131.
- Tarp-Johansen, M.J., 2002. Stem diameter estimation from aerial photographs, *Scandinavian Journal of Forest Research*, 17:369–376.
- Tsanis, I.K., and K. Seiradakis, 2002. *Application of New Technologies in Water Resources Management in the Keritis Hydrological Basin*, Masters thesis, Technical University of Crete, Department of Environmental Engineering, (in Greek).
- Tsanis, I.K., K. Seiradakis, and M. Apostolaki, 2006. Satellite RS as a tool for agricultural and water resources management, *Proceedings of the 2nd Workshop of the EARSel SIG on Land use & Land cover*, Bonn, Germany.

(Received 01 June 2008; accepted 01 November 2008; revised 05 January 2009)